

DCC formation and observation in nucleus-nucleus collisions

Jørgen Randrup^{a*}

^aNuclear Science Division, Lawrence Berkeley National Laboratory,
University of California, Berkeley, California 94720

High-energy nucleus-nucleus collisions may produce extended regions of space within which chiral symmetry is temporarily nearly restored. The subsequent non-equilibrium relaxation towards the normal vacuum may then produce *disoriented chiral condensates*: isospin-directed oscillations of the pion field. The conditions for the occurrence of this novel phenomenon and some of its observational consequences are discussed.

1. INTRODUCTION

Nucleus-nucleus collisions are generated in laboratories around the world for the purpose of bringing the nuclear system far away from its ordinary tranquil state and thus make it possible to explore novel aspects of its physical properties. As ever more powerful accelerators (and increasingly refined detector systems) are becoming available, the scope of these studies has steadily expanded. Not only has the accessible domain of the nuclear chart grown explosively, but prospects have appeared for probing fundamental features of strongly interacting systems. In particular, a long-standing goal has been to probe the non-perturbative properties of QCD and the expected transition to a deconfined quark-gluon plasma phase. Of somewhat more recent date is the recognition that high-energy nucleus-nucleus collisions may also provide key insights into chiral symmetry: the collision may produce extended regions of space within which chiral symmetry is temporarily nearly restored and the subsequent non-equilibrium relaxation towards the normal vacuum may then produce large-amplitude coherent oscillations of the pion field, *disoriented chiral condensates*, which will lead to an enhanced emission of isospin-polarized soft pions [1–6]. This presentation seeks to provide simple and instructive insight into the key features of this novel phenomenon, the conditions for its actual occurrence in nuclear collisions, and the prospects for its experimental detection. (For a recent review, see ref. [7].)

2. EQUILIBRIUM

A suitable model framework is presented by the linear σ model, within which the emergence of coherent long-wavelength oscillations in the pion field has been studied by a number of investigators in a variety of idealized scenarios. (For some of the earliest dynamical studies, see refs. [8–13].)

*Work supported by the Director, Office of Energy Research, Office of High Energy and Nuclear Physics, Nuclear Physics Division of the U.S. Department of Energy under Contract No. DE-AC03-76SF00098.

The linear σ model describes the degrees of freedom associated with the isoscalar σ field and the isovector $\boldsymbol{\pi}$ field. These are conveniently combined into the (real) $O(4)$ field $\boldsymbol{\phi}$ which has a non-linear equation of motion,

$$\boldsymbol{\phi}(\mathbf{r}, t) = (\sigma(\mathbf{r}, t), \boldsymbol{\pi}(\mathbf{r}, t)) , \quad \left[\square + \lambda(\phi^2 - v^2) \right] \boldsymbol{\phi} = H \hat{\sigma} , \quad (1)$$

where the three model parameters, λ , v , and H , can be fixed by specifying the pion decay constant f_π and the two meson masses, m_π and m_σ . The vacuum field is aligned with the σ direction, $\boldsymbol{\phi}_{\text{vac}} = (f_\pi, \mathbf{0})$, and at low temperatures the field fluctuations represent nearly free σ and π mesons.

Instructive insight into the DCC phenomenon can be gained by decomposing the chiral field into a smooth part, the *order parameter*, and the fluctuations around it, representing the *quasi-particles*, $\boldsymbol{\phi}(\mathbf{r}, t) = \underline{\boldsymbol{\phi}}(t) + \delta\boldsymbol{\phi}(\mathbf{r}, t)$. In the present discussion we shall confine the field to a rectangular box with periodic boundary conditions and the decomposition can then be made in a unique manner ($\underline{\boldsymbol{\phi}}$ is then simply the spatial average $\langle \boldsymbol{\phi} \rangle$), but generally it needs to be done locally so $\underline{\boldsymbol{\phi}}$ itself may vary with position.

By taking the spatial average of the full equation of motion (1), it is possible to derive an equation of motion for the order parameter [14]. If we subsequently subtract that from (1) and apply a Hartree-type factorization, we obtain corresponding equations for the field fluctuations [15]. The resulting equations of motion are then of mean-field form,

$$\left[\square + \mu_0^2 \right] \underline{\boldsymbol{\phi}} = H \hat{\sigma} , \quad \mu_0^2 = \lambda [\phi_0^2 + \langle \delta\phi^2 \rangle + 2\langle \delta\phi_{\parallel}^2 \rangle - v^2] , \quad (2)$$

$$\left[\square + \mu_{\parallel}^2 \right] \delta\phi_{\parallel} = 0 , \quad \mu_{\parallel}^2 = \lambda [3\phi_0^2 + \langle \delta\phi^2 \rangle + 2\langle \delta\phi_{\parallel}^2 \rangle - v^2] , \quad (3)$$

$$\left[\square + \mu_{\perp}^2 \right] \delta\phi_{\perp} = \mathbf{0} , \quad \mu_{\perp}^2 = \lambda [\phi_0^2 + \langle \delta\phi^2 \rangle + 2\langle \delta\phi_{\perp}^2 \rangle - v^2] . \quad (4)$$

Here $\delta\phi_{\parallel} = \delta\boldsymbol{\phi} \circ \hat{\boldsymbol{\phi}}$ is the fluctuation along the order parameter and $\delta\phi_{\perp}$ is the fluctuation perpendicular to $\underline{\boldsymbol{\phi}}$. Furthermore, we have for simplicity ignored the cross terms arising from correlations between field fluctuations in different $O(4)$ directions (they vanish in equilibrium). When those are retained as well, the resulting mean-field description is analogous to the collisionless Vlasov model familiar from the description of nuclear dynamics at intermediate energies [16].

The mean-field approximation is particularly useful for achieving an approximate description of thermal equilibrium. The spatial averages $\langle \cdot \rangle$ are then replaced by the corresponding thermal averages $\prec \cdot \succ$, evaluated at the given temperature T ,

$$\prec \delta\phi_{\parallel}^2 \succ = \frac{1}{\Omega} \sum'_{\mathbf{k}} \frac{\prec n_{\mathbf{k}}^{\parallel} \succ}{\epsilon_{\mathbf{k}}^{\parallel}} , \quad \prec n_{\mathbf{k}}^{\parallel} \succ = (e^{\epsilon_{\mathbf{k}}^{\parallel}/T} - 1)^{-1} , \quad \epsilon_{\mathbf{k}}^{\parallel} = (k^2 + \mu_{\parallel}^2)^{\frac{1}{2}} , \quad (5)$$

$$\prec \delta\phi_{\perp}^2 \succ = \frac{1}{\Omega} \sum'_{\mathbf{k}} \frac{\prec n_{\mathbf{k}}^{\perp} \succ}{\epsilon_{\mathbf{k}}^{\perp}} , \quad \prec n_{\mathbf{k}}^{\perp} \succ = (e^{\epsilon_{\mathbf{k}}^{\perp}/T} - 1)^{-1} , \quad \epsilon_{\mathbf{k}}^{\perp} = (k^2 + \mu_{\perp}^2)^{\frac{1}{2}} . \quad (6)$$

The volume of the box is given by Ω and $\mathbf{k} \neq 0$ denotes the wave vector of the individual quasi-particle modes in the cavity. We note that the effective masses increase with the magnitude of the order parameter ϕ_0 as well as with the field fluctuations. They are degenerate for $\phi_0=0$ and vanish at the “critical” temperature $T_c = \sqrt{2}v$. Moreover, we always have $\mu_0^2 \leq \mu_{\perp}^2 \leq \mu_{\parallel}^2$.

It is then possible to derive the corresponding expression for the partition function associated with the chiral field,

$$\mathcal{Z}_T = \int \mathcal{D}[\underline{\psi}, \underline{\phi}] e^{-\frac{\Omega}{T} E[\underline{\psi}, \underline{\phi}]} = \int d^4 \underline{\psi} d^4 \underline{\phi} W_T(\underline{\psi}, \underline{\phi}), \quad W_T(\underline{\psi}, \underline{\phi}) \approx e^{-\frac{\Omega}{T} (K_0 + V_T - T S_T)}, \quad (7)$$

where $\underline{\psi}$ denotes the time derivative of the field $\underline{\phi}$ and plays the role of its conjugate momentum. The statistical weight W_T gives the relative probability for finding the system with a specified value of the order parameter $\underline{\phi}$ and its time derivative $\underline{\psi}$. Its simple approximate form contains the kinetic energy density of the order parameter $K_0 = \dot{\phi}_0^2/2$, the effective potential energy density V_T , and the entropy density S_T associated with the quasi-particle degrees of freedom for a given value of ϕ_0 . The corresponding free energy $F_T = V_T - T S_T$ can be expressed explicitly,

$$F_T(\underline{\phi}) = \frac{\lambda}{4} (\phi_0^2 - v^2)^2 - H \phi_0 \cos \chi_0 + \frac{T}{\Omega} \sum_{\mathbf{k}}' [\ln(1 - e^{-\epsilon_{\mathbf{k}}^{\parallel}/T}) + 3 \ln(1 - e^{-\epsilon_{\mathbf{k}}^{\perp}/T})] \\ - \frac{3}{4} \lambda [\chi \delta \phi_{\parallel}^2 \chi^2 + 2 \chi \delta \phi_{\parallel}^2 \chi \chi \delta \phi_{\perp}^2 + 5 \chi \delta \phi_{\perp}^2 \chi^2]. \quad (8)$$

The free energy is shown in Fig. 1. At high temperature, its minimum is located near the origin and chiral symmetry is thus approximately restored. As T is decreased, the accompanying reduction of the field fluctuations causes the free energy to gradually change its appearance, with its minimum moving steadily outwards towards the vacuum value. Figure 2 shows the corresponding temperature dependence of the effective quasi-particle masses. Starting out at its free value m_{π} for $T=0$, the pion mass grows steadily with T , whereas the σ mass first experiences a significant dip (the minimum occurs at $T_{\chi} \approx 240$ MeV), before turning upwards and becoming nearly degenerate with the pion mass, as approximate chiral symmetry is attained at high T .

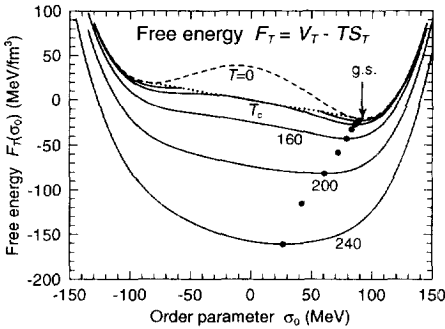


Figure 1. The free energy F_T as a function of the order parameter (along the σ axis) for a number of temperatures T between zero and 240 MeV. The solid dots highlight the equilibrium values.

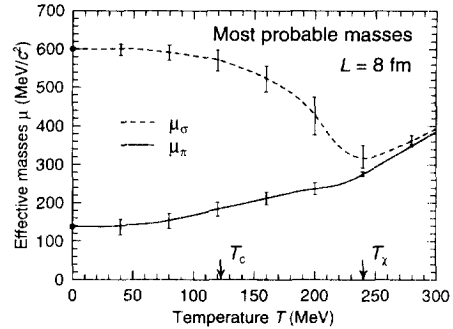


Figure 2. The effective masses μ_{π} and μ_{σ} for a thermal ensemble of field configurations in a cubic box with $L=8$ fm. The error bars show the effect of the thermal fluctuations of the order parameter.

3. DYNAMICS

Since the interesting DCC dynamics proceeds far from equilibrium, it is important to develop some means of capturing and depicting the essential features of an arbitrary field configuration. This can be done by invoking the field decomposition mentioned above and employ a “chiral phase diagram” which adopts the magnitude of the order parameter as the abscissa and the field dispersion as the ordinate. Thus any given chiral field configuration $\phi(\mathbf{r}, t)$ projects onto the point $(\phi_0, \Delta\phi)$, with $\phi_0^2 = \phi \circ \phi$ and $\Delta\phi = \langle \delta\phi^2 \rangle^{1/2}$. The field dispersion is a convenient general indicator of the degree of agitation in the system and in thermal equilibrium it is related to the temperature T .

Figure 3 shows the most important landmarks on the chiral phase diagram: the location of the thermal equilibria and the region within which the soft quasi-pions are unstable. The equilibrium values of the order parameter are those associated with the minima in the free energy shown in Fig. 1. We note that the transition from the ordinary broken to the approximately restored phase occurs as a smooth crossover for $T \approx 180 - 240$ MeV. The minimum of the σ mass, which occurs within this range, is a convenient indicator of the effective transition temperature [17] (shown as $T_\chi \approx 240$ MeV in Fig. 2).

As is evident from Eq. (4), the square of the effective quasi-pion mass is negative in the lower-left region of the chiral diagram, where both the order parameter and the field fluctuations are small. Consequently, if the system enters this region, an exponential amplification will be experienced by those pion modes for which $\omega_k^2 \equiv k^2 + \mu_\perp^2$ is negative. This unstable region is delineated by an approximately parabolic curve which intersects the abscissa at $\phi_0 = v$, somewhat below the ground-state value f_π . Moreover, the critical boundary curve reaches $\phi_0=0$ when $\Delta\phi^2 = \frac{2}{3}v^2$, obtained at the “critical” temperature $T_c = \sqrt{2}v \approx 122$ MeV for which the effective masses μ_\parallel and μ_\perp both vanish.

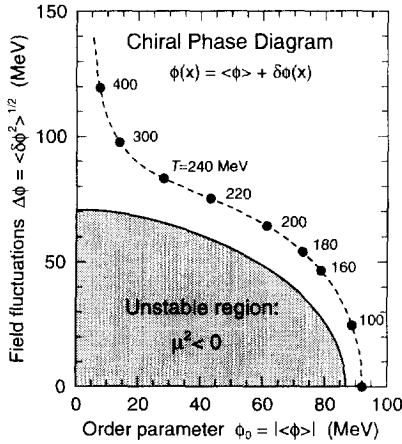


Figure 3. The chiral phase diagram. The thermal equilibria are joined by the dashed curve and the region within which the soft pion modes are unstable is shaded.

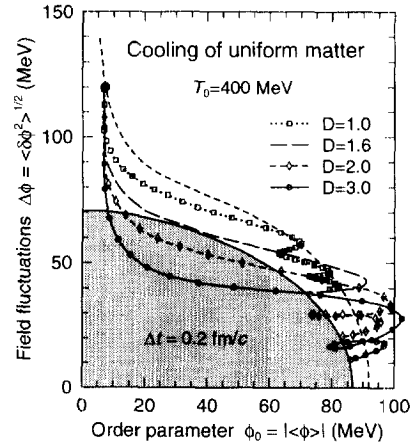


Figure 4. Dynamical trajectories of systems prepared at $T_0=400$ MeV and then subjected to a Rayleigh-type cooling emulating scaling expansion in D dimensions.

The nucleus-nucleus collision is expected to generate a high degree of agitation in the chiral field and thereby induce an approximate restoration of chiral symmetry. Thus, the early field configuration is located somewhere in the upper-left region of the chiral diagram shown on Fig. 3. Subsequently, the field fluctuations will rapidly subside, as the combined result of expansion, radiation, and a possible supercooling [18,19]. This, in turn, will modify the free energy (see Fig. 1) and thus cause the order parameter to grow. The emerging dynamical path on the chiral diagram will then be determined by the balance between the effective cooling rate and the relaxation of the order parameter towards its vacuum value.

An instructive impression of the time scales involved can be gained by studying the response of the system to an imposed rate of cooling. For this purpose, it is convenient to add the term $-(D/t)\partial_t$ on the right-hand side of the equation of motion (1) for ϕ , since that approximately emulates the effect of a Bjorken-type scaling expansion in D spatial dimensions [20]. The result is illustrated in Fig. 4. It appears that a purely longitudinal expansion, $D=1$, is insufficient for bringing the system into unstable region, which is in accordance with earlier simulations [12,21]. Thus, if a sufficient quench is to be produced by expansion alone, it is evident that a considerable amount of transverse expansion is required as well.

The condition for the dynamical development of a quench can be quantified by considering the characteristic time scale for the cooling, $t_{\text{cool}} \equiv -E/\dot{E} \approx t/D$. Then $D=1$ translates into $t_{\text{cool}} = t_0$ at the time at which the system is started off (usually taken as $t_0 = 1$ fm/c). Thus, in order to surpass the critical value $D > 1.6$ (see Fig. 4), t_{cool} must be shorter than about 0.6 fm/c. Results obtained with the parton cascade model for central collisions of gold nuclei at RHIC energies [22] suggest an effective value of $D_{\text{eff}} \approx 1.15$ which would thus be too small to bring the system inside the unstable region. It is obviously important to make a refined estimation of this key quantity, since it has a decisive bearing on the prospects for the occurrence of disoriented chiral condensates.

4. OBSERVABLES

While awaiting the outcome of such further investigations, let us assume that the dynamics of the nucleus-nucleus collision does in fact produce a sufficiently rapid quench to force the system through the region where the soft pion modes are being amplified. We may then turn to the question of how this will be manifested in the observables. In order to illustrate the discussion by specific results, we shall concentrate on scenarios corresponding to an intermediate cooling rate, $D=2$.

We first note that the Rayleigh cooling causes the field fluctuations to fall off as $\delta\phi \sim t^{-D/2}$ at large times, so that the energy density drops as $\sim t^{-D}$, like in a scaling expansion in D dimensions. Thus, the decoupled linear regime is approached where the field may be represented as a superposition of uncoupled plane waves having a complex frequency, $\omega_k \approx \epsilon_k - i\gamma$ with $\gamma = D/2t$.

Furthermore, for notational convenience, the real field $\phi(x, t) = \sum_k \phi_k \exp(ikx)$ and its time derivative $\psi(x, t) = \sum_k \psi_k \exp(ikx)$ may be combined into the complex field $\chi(x, t) = \sum_k \chi_k \exp(ikx)$ where $\chi_k \equiv (\epsilon_k/2)^{1/2} \phi_k + i(2\epsilon_k)^{-1/2} \psi_k$. For large times we then have $\dot{\chi}_k = -i\omega_k \chi_k$, except for small higher-order terms in the time dependence of γ .

In order to calculate observable quantities, it is necessary to associate the chiral field χ , the quantity that is propagated dynamically, with a specific quantum many-body state, $|\chi\rangle$. This can be done by means of a coherent state and we make the association

$$\chi \longrightarrow |\chi\rangle \sim \exp\left[\sum_k \chi_k \hat{a}_k^\dagger\right] |0\rangle, \quad (9)$$

where \hat{a}_k denotes the quasi-particle annihilation operator. The coherent state $|\chi\rangle$ does not have a definite particle number. Rather, the multiplicity of particles in a given mode k is a Poisson distribution characterized by the mean value $\bar{n}_k \equiv \langle \chi | \hat{a}_k^\dagger \hat{a}_k | \chi \rangle = \chi_k^* \chi_k$. Thus it is possible to extract any hadronic observables of interest. (Since the generalization is straightforward, the above sketch is made for the simplest case possible: only one spatial and one internal dimension and without any special isospin correlations imposed.)

4.1. Pion power spectrum and correlation function

Figure 5 shows the resulting power spectrum of the emerging pions, as a function of their kinetic energy, $P_\pi(E_{\text{kin}}) \sim \sum_{\mathbf{k}} \epsilon_k^2 |\chi_{\mathbf{k}}|^2 \delta(E_{\text{kin}} + m_\pi - \epsilon_k)$, as explained above. There is a clear enhancement at the lowest kinetic energies, of the type discussed in ref. [23]. There is no such enhancement for $D=1$, whereas $D=3$ produces a significantly larger enhancement of the soft part of the pion spectrum [16].

This non-equilibrium feature has an important effect on the pion correlation function $C_\pi(r_{12}) = \langle \boldsymbol{\pi}(\mathbf{r}_1) \cdot \boldsymbol{\pi}(\mathbf{r}_2) \rangle$. The increased strength of the softest pion modes causes C_π to acquire a pronounced tail, as shown in Fig. 6. While the correlation function retains an approximately thermal form for $D=1$, it widens steadily for larger cooling rates [16].

Moreover, since the order parameter is initially small, its initial development is primarily a radial growth in the chiral $O(4)$ space, until $\phi_0 \approx f_\pi$ has been reached. Thus, there is practically no rotational motion generated and its subsequent oscillations are well directed in isospace. (The instability affects only the axial vector current density, so that the vector current density remains small.) The essential effect of the quench is thus the establishment of “domains” within which the pion field exhibits long-wavelength large-amplitude oscillations in a definite isospin direction.

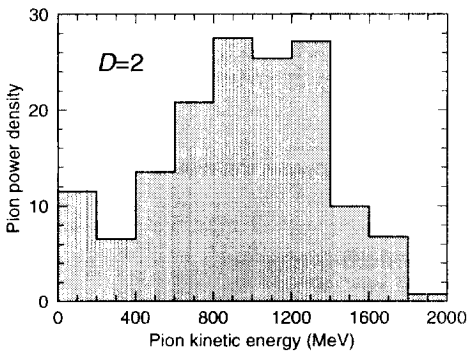


Figure 5. The pion power spectrum after the non-equilibrium cooling with $D=2$ (Fig. 4).

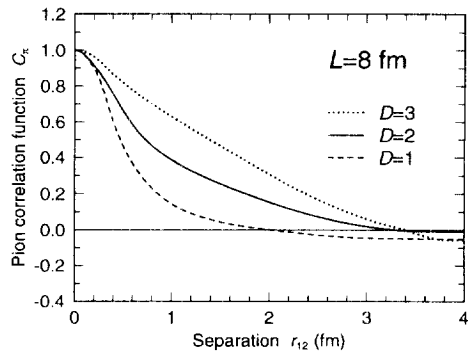


Figure 6. The pion correlation function after cooling with $D=1,2,3$ as in Fig. 4.

4.2. Neutral pion fraction

It was noted early on that isospin-directed oscillations of the pion field will result in an anomalous behavior of the neutral pion fraction $f = n_{\pi_0}/n_{\pi}$ [1–6]. Indeed, the distribution would be given by $P(f) = 1/(2\sqrt{f})$ in the idealized scenario where all the pions observed arise from a fully aligned source. In practice, the observed pions may originate from unrelated regions and the anomaly is then attenuated. This is illustrated in Fig. 7 which shows the result of combining pions from N independent sources. A usual Poisson-like distribution peaked near $f = \frac{1}{3}$ emerges when there are many independent sources, or equivalently, when the distance between emission points is large in comparison with the correlation length.

In order to give a quantitative feeling for what this inherent feature amounts to in practice, we show in Fig. 8 the distribution $P(f)$ extracted from an ensemble of 100 events that have been cooled with $D=2$, as explained above. When all the pions are used for the calculation of f , the resulting distribution looks fairly normal, but when only pions with a kinetic energy below 200 MeV are considered, then $P(f)$ broadens significantly and attains an anomalous form. However, its appearance still differs significantly from the ideal form, which is only reached if all the pions arise from a single mode, such as the one having $k=0$.

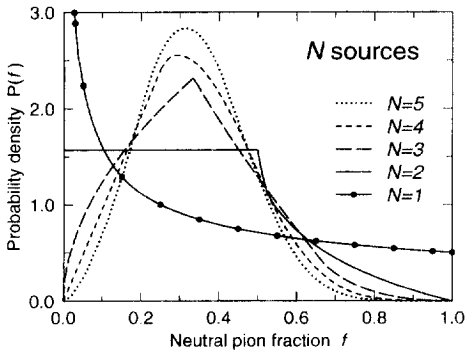


Figure 7. The neutral fraction distribution $P(f)$ resulting from N similar sources having independent isospin alignments.

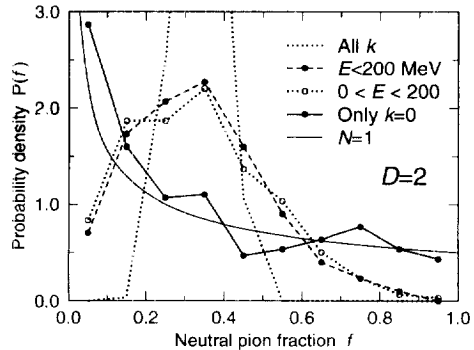


Figure 8. The distribution $P(f)$ when various energy cuts are applied, as extracted from an ensemble obtained with $D=2$.

This important feature can also be brought out by viewing a given source at different scales, as illustrated in Fig. 9 where the total source is divided into ever smaller sources, each one leading to a separate value of f . As the source size shrinks, its pion field is increasingly well aligned and the associated $P(f)$ grows correspondingly more anomalous. (For wavelet-type analyses of DCC domain structure, see refs. [24–26].)

The key quantity determining the form of the extracted $P(f)$ is the pion correlation length. In the examples above, the growth of the correlation length was caused by the non-equilibrium evolution following a quench. However, a large correlation length can also exist in thermal equilibrium, since it grows steadily as T is reduced, and thus similar

results can be produced by a thermal source, as is illustrated in Fig. 10. Therefore, the appearance of an anomalous neutral pion fraction distribution is not a unique signal of the DCC phenomenon. More elaborate analyses are thus required and it may be preferable to invoke several different observables. In particular, electromagnetic observables, namely dileptons [27,28] and photons [29], may provide valuable additional information.

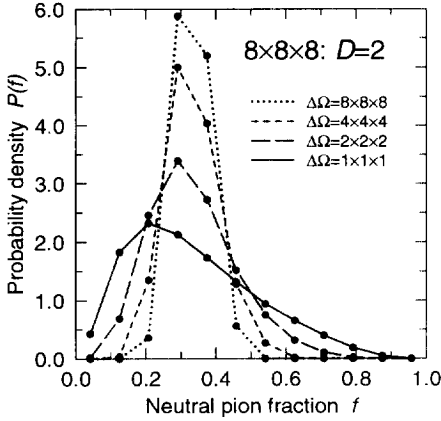


Figure 9. $P(f)$ for a cube with $L=8$ fm that has been cooled with $D=2$ and then subdivided into ever smaller cubic sources [23].

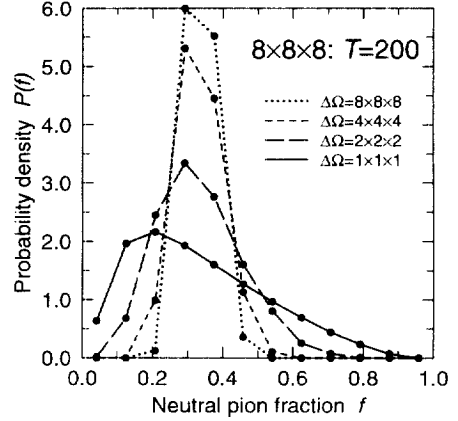


Figure 10. $P(f)$ for a cube prepared in equilibrium at $T=200$ MeV and then subdivided into ever smaller cubic sources.

4.3. Electromagnetic signals

The non-equilibrium DCC evolution following a quench was recently found to enhance the photoproduction significantly and it was suggested that this effect may provide an experimental signature for the formation and relaxation of DCCs in nucleus-nucleus collisions [29]. Furthermore, long-wavelength pionic oscillations and their interaction with the thermal environment can be a significant source of dileptons and recent studies [28] suggest that the yield of dileptons with invariant mass near and below $2m_\pi$ may be enhanced by up to two orders of magnitude.

This latter feature is illustrated below. Once the field evolution is known, the invariant differential rate for dilepton production can be expressed in terms of the electromagnetic current density, $J_\mu(x) = \pi_1(x)\partial_\mu\pi_2(x) - \pi_2(x)\partial_\mu\pi_1(x)$, as

$$\frac{d^4N}{d^4q} = \frac{2}{3\pi} \left(\frac{\alpha}{2\pi}\right)^2 \left(\frac{q^\mu q^\nu}{q^4} - \frac{g^{\mu\nu}}{q^2} \right) \int d^4x \int d^4y J_\mu(x) e^{-iq(x-y)} J_\nu(y), \quad (10)$$

for each individual event. An average over an ensemble of individual evolutions can then be made subsequently, as is done experimentally.

It is reassuring to note that if such an average is made over a thermal ensemble of free-field evolutions, then the usual expression for production of dileptons with invariant

mass M by pion annihilation is recovered exactly [28],

$$\left\langle \frac{d^4 N}{d^4 q d^4 x} \right\rangle = \frac{\alpha^2}{3} \frac{n_0^2}{(2\pi)^4} \left(1 - \frac{4m_\pi^2}{M^2} \right)^{\frac{3}{2}}, \quad (11)$$

where n_0 is the thermal occupancy of pion states with the matching energy $\epsilon_0 = M/2$.

Figure 11 shows the dilepton production rate in a source in thermal equilibrium at $T=140$ MeV, together with the corresponding result obtained when the system is prepared in a quenched configuration where nearly all the thermal energy (about 40 MeV/fm³) has been converted into potential energy of the displaced order parameter [28]. As is shown in Fig. 12, the release of the system causes the order parameter to execute large oscillations around its equilibrium value leading to a significant enhancement of the dileptons. In addition to the amplification that occurs whenever the system is inside the unstable region, as discussed above, there is an additional enhancement resulting from the parametric amplification caused by the approximately regular oscillation of the order parameter with a frequency near the σ mass [28,29]. Although only rather schematic scenarios have been considered so far, the large magnitude of the enhancement should provide a stimulus for more refined studies.

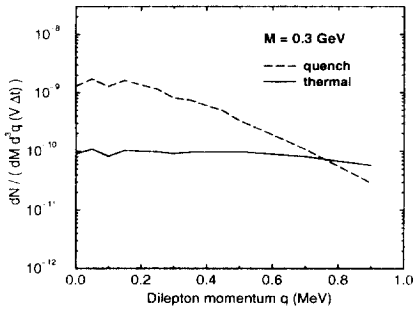


Figure 11. The dilepton production rate $d^4 N/(d^4 q d^4 x \Delta t)$ as a function of the magnitude of the dilepton momentum, for dilepton masses near $M=300$ MeV [25].

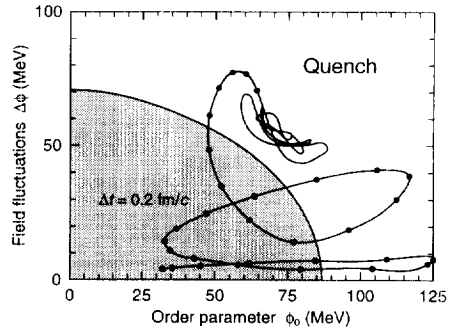


Figure 12. The dynamical path of the field, as projected onto the chiral diagram, for the quench scenario employed for the dilepton calculation shown in Fig. 11.

5. CONCLUDING REMARKS

The present discussion has been concerned with the conditions for the occurrence of disoriented chiral condensates and the possible observational implications. The essential features of a large body of dynamical simulations with the linear σ model can be understood within the simple framework of a semi-classical Hartree treatment. The studies suggest that a sufficiently rapid quench can only be expected if the cooling rate is faster than what is provided by an idealized longitudinal scaling expansion. A more definite

assessment will require refined dynamical calculations that take better account of the three-dimensional geometry as well as the additional degrees of freedom in the system.

If indeed the collision dynamics leads to DCC formation, then the experimental identification of the phenomenon presents a daunting task. The most prominent hadronic signal, the neutral fraction distribution, requires the simultaneous detection of both charged and neutral soft pions. Moreover, the magnitude of the signal depends on the ability to zoom in on small source sizes. As for electromagnetic observables, the exploratory studies suggest that large enhancements may occur. For all the possible DCC signals, it is important to investigate how they are affected (presumably adversely) by the environment generated in the nucleus-nucleus collision.

The author acknowledges helpful discussions with Xin-Nian Wang and wishes to thank Wolfgang Bauer and Ramona Vogt for their reading of the manuscript.

REFERENCES

1. A.A. Anselm, Phys. Lett. B217 (1989) 169.
2. A.A. Anselm and M.G. Ryskin, Phys. Lett. B266 (1991) 482.
3. J.D. Bjorken, K.L. Kowalski, and C.C. Taylor, SLAC-PUB-6109 (1993).
4. J.D. Bjorken, K.L. Kowalski, and C.C. Taylor, *hep-ph/9309235*.
5. K. Rajagopal and F. Wilczek, Nucl. Phys. B399 (1993) 395.
6. J.P. Blaizot and A. Krzywicki, Phys. Rev. D46 (1992) 246.
7. J.P. Blaizot and A. Krzywicki, Acta Phys. Polon. 27 (1996) 1687.
8. K. Rajagopal and F. Wilczek, Nucl. Phys. B404 (1993) 577.
9. S. Gavin, A. Gocksch, and R.D. Pisarski, Phys. Rev. Lett. 72 (1994) 2143.
10. S. Gavin and B. Müller, Phys. Lett. B329 (1994) 486.
11. J.P. Blaizot and A. Krzywicki, Phys. Rev. D50 (1994) 442.
12. Z. Huang and X.N. Wang, Phys. Rev. D49 (1994) 4335.
13. F. Cooper, Y. Kluger, E. Mottola, and J.P. Paz, Phys. Rev. D51 (1995) 2377.
14. G. Baym and G. Grinstein, Phys. Rev. D15 (1977) 2897.
15. J. Randrup, Phys. Rev. D55 (1997) 1188.
16. J. Randrup, Nucl. Phys. A616 (1997) 531.
17. R.D. Pisarski, Phys. Rev. D52 (1995) R3773.
18. L.P. Csernai and I.N. Mishustin, Phys. Rev. Lett. 74 (1995) 5005.
19. S. Mrowczynski and B. Müller, Phys. Lett. B363 (1995) 1.
20. J. Randrup, Phys. Rev. Lett. 77 (1996) 1226.
21. M. Asakawa, Z. Huang, and X.N. Wang, Phys. Rev. Lett. 74 (1995) 3126.
22. K. Geiger and J.I. Kapusta, Phys. Rev. D47 (1993) 4905.
23. S. Gavin, Nucl. Phys. A590 (1995) 163c.
24. Z. Huang, I. Sarcevic, R. Thews, and X.N. Wang, Phys. Rev. D54 (1996) 750.
25. K. Rajagopal, Hirschegg Winter Workshop XXV (1997); *hep-ph/9703258*.
26. J. Randrup and R.L. Thews, Phys. Rev. D (in press); *hep-ph/9705260*.
27. Z. Huang and X.N. Wang, Phys. Lett. B383 (1996) 457.
28. Y. Kluger, V. Koch, J. Randrup, and X.N. Wang, PRC (in press); *nucl-th/9704018*.
29. D. Boyanovsky, H.J. de Vega, R. Holman, and S. Prem Kumar, PRD; *hep-ph/9701360*.